Analyst

COMMUNICATION

View Article Online
View Journal

Cite this: DOI: 10.1039/c6an02080a

Received 16th September 2016,
Accepted 15th November 2016

DOI: 10.1039/c6an02080a

www.rsc.org/analyst

A protocol for rapid, label-free histochemical imaging of fibrotic liver

B. Bird* and J. Rowlette

Mid-infrared microscopy is a non-destructive, quantitative and label-free spectroscopic imaging technique that, as a result of recent instrument advancements, is now at the point of enabling high-throughput automated biochemical screening of whole histology samples. Currently the mid-infrared field is undergoing a paradigm shift that has not been seen since the introduction of scanning Fourier Transform interferometric spectrometers. The latest mid-infrared microscopes are powered by tunable quantum cascade laser (QCL) sources which offer a number of advantages including measurement protocol flexibility, ease-of-use and a greatly enhanced data acquisition speed at high spectral and spatial resolution. In this study we use a wide-field QCL infrared microscope to develop and validate a fast four-frequency protocol for imaging fibrosis in unstained liver tissue. We compare our results to the gold standard Masson's trichrome histochemical staining protocol.

Introduction

The diagnostic evaluation of liver tissue is most commonly achieved *via* the exhaustive microscopic evaluation of tissue sections stained with Haematoxylin and Eosin (H&E). Dependent on initial findings, the clinical/patient background, and the preference of the pathologist, additional special stains may be used to identify tissue features that are not easily discernible *via* conventional H&E staining. The Masson's trichrome stain is the most common special stain used for liver specimen screening.[1] The stain imparts a blue colour to collagen against a red background of hepatocytes and other structures. It more specifically stains type 1 collagen, which is normally present in healthy samples within the portal tracks and vessel walls. But its most predominant use is to highlight and track the distribution of reactive fibrosis as a result of liver injury, and is used to stage chronic liver diseases, including cirrhosis.

Daylight Solutions Inc., 15378 Avenue of Science, Suite 200, San Diego, CA 92128, USA. E-mail: b.bird@daylightsolutions.com

Collagen has several characteristic vibrational bands across the mid-infrared spectrum,[2–7] most notably in the low wavenumber region with a triad of peaks in the Amide III region centred at 1232 cm^{-1}, with shoulder bands at 1204 and 1280 cm^{-1} respectively. Unfortunately, several other molecules have overlapping peaks in this region, such as the antisymmetric phosphate stretches of nucleic acids and phospholipids. However, the small band centred at 1336 cm^{-1} arising from collagen CH_2 side-chain vibrations has less overlap and has been shown to provide excellent contrast for collagen deposition in heart tissue following myocardial infarction.[4] This band was also found to be highly indicative of collagen in synchrotron generated infrared maps of liver tissue when directly compared to immunofluorescence microscopy using the monoclonal anti-collagen III antibody.[5]

More recently, fibrillar collagen scoring by second-harmonic generation microscopy, coupled with two-photon or multiphoton autofluorecence microscopy, has been reported. These investigations report automated algorithms that provide quantitative measures that correlate to the conventional METAVIR (fibrosis) scoring system, but have yet to translate into mainstream pathology.[8–10] This in part may be due to its limited applicability, providing sensitivity to highly ordered structures without symmetry in tissue alone, namely collagen type I. Mid-infrared spectroscopy, however, provides additional advantages since it is sensitive to the structure of all cellular components, and can provide information regarding protein, lipid, nucleic acid and carbohydrate composition simultaneously.

The periodic acid-Schiff(PAS) stain is another special stain useful to identify the presence of glycogen in tissue.[1] Identification of glycogen as globules in hepatocytes is a marker for various glycogen storage diseases,[1,11,12] including von Gierke's disease for example.

Glycogen also has several characteristic bands in the low wavenumber region of the spectrum, at 1028 (COH deformation), 1080 (C–C stretch) and 1152 (C–O stretch) cm^{-1} respectively.[2,13] Mucin glycosylation bands, with similar peak positions were recently used to replicate PAS staining of

colonic tissue from mice, by collecting data from a reduced wavelength range.[14]

This contribution presents a protocol for high-contrast imaging of fibrotic tissue structures in unstained biopsied cirrhotic liver tissue specimens. This example serves as a case study in support of rapid mid-IR screening of reactive fibrosis in organs. Increased speed was achieved by targeting only a small number of salient mid-infrared frequencies associated with collagen.

Materials and methods

Sample preparation

Liver tissue sections were cut from archival tissue banks of formalin fixed paraffin embedded (FFPE) tissue blocks (SDPathology, San Diego, USA). Three parallel sections were cut from each sample for analysis. The first section was cut at 5 μm thickness and floated onto a regular glass slide for H&E staining. The second section was cut at 10 μm thickness and floated onto a CaF_2 disc (25 mm × 2 mm) for infrared microscopy. The third section was cut at 5 μm thickness and floated onto a regular glass slide for Masson trichrome staining. All sections were de-paraffinised and stained using standard protocols.[15,16] Deparaffinisation included the following steps: (a) immersion in xylene for 10 minutes (b) immersion in a fresh batch of xylene for 10 minutes (c) immersion in 100% ethanol for 5 minutes (d) immersion in 95% ethanol for 5 minutes (e) immersion in 70% ethanol for 5 minutes (f) rinse in distilled water for 5 minutes. The sections mounted onto glass were subsequently cover slipped before conventional brightfield imaging at 20× magnification using a whole slide imaging system (Hamamatsu, Japan). The section mounted onto CaF_2 disc remained stain-free and stored in a desiccator prior to infrared microscopy.

QCL-based infrared microscopy

QCL-based infrared microscopy[7,14,17–20] was performed using a Spero microscope (Daylight Solutions Inc., San Diego, USA). High definition mosaic images were recorded from the tissue samples using the 12.5×, 0.7 N.A., compound refractive infrared objective of the microscope. This optic has a field of view 650 μm × 650 μm (480 × 480 pixels), and sample referenced pixel size of 1.35 μm. Wide-field mosaic images were recorded from the tissue samples using the 4×, 0.3 N.A., compound refractive infrared objective of the microscope. This optic has a field of view 2000 μm × 2000 μm (480 × 480 pixels), and sample referenced pixel size of 4.25 μm. Infrared images were either recorded from the full fingerprint region between 900–1800 cm^{-1}, or from a reduced set of 4 sparsely distributed frequencies within the same region, located at 1140, 1232, 1336, and 1356 cm^{-1} respectively. These frequencies were selected after consultation of several rigorous FT-IR based studies performed by multiple independent research groups[2–7] and our preliminary findings as reported below in the results and discussion section. Briefly, strong spectral bands are observed for collagen rich tissue at 1232 and 1336 cm^{-1} respectively. The results observed are comparable to those of Chehelatani *et al.* and K. Lui *et al.*[4,5] that reported a strong correlation of the 1336 cm^{-1} band to the presence and staining of collagen. All tissue types found in the liver samples provided a spectral band at 1232 cm^{-1}, but the collagen rich tissues alone provide a specific and more pronounced spectral band at 1336 cm^{-1}, with little overlap from additional bands. Thus, a ratio of these two characteristic bands is sensitive to the collagen concentration at any discrete spatial location, and should be insensitive to small fluctuations that may occur in tissue thickness and density. Absorbance intensities were recorded at two additional frequencies (1356 and 1140 cm^{-1}) to allow the subtraction of a linear baseline from the measurements and minimize variance from baseline distortions caused by scattering. Each spectral hypercube took 5 minutes for a full broadband spectrum and 0.3 minutes for a sparse frequency data collection. The data was recorded at 8 cm^{-1} spectral resolution with a 4 cm^{-1} data interval, and ratioed against a background from a clean area of the substrate. Spectral hypercubes 480 × 480 × 226 (102 MB) or 480 × 480 × 4 (2 MB) were thus created.

Data pre-processing

Raw data sets were imported into the multisensor imaging software package ImageLab.[21] The data processing included:

- Noise reduction *via* the maximum noise fraction transform[22]
- Spectral quality test to remove pixel spectra from regions not occupied by tissue
- Full band spectra were baseline corrected using an asymmetric least squares approach (Eilers algorithm, 5 iterations)[23]
- Full band spectra were min–max normalised using the Amide I band to reduce the influence of intensity changes caused by differences in cellular density and tissue thickness.
- Sparse frequency datasets were used to calculate peak height ratio values as follows: the logarithm of the ratio of two peak intensities at two different wavelengths weighted by the intensity of the second peak. The peak intensities are measured relative to a baseline which is obtained from two reference points.

This approach is an implementation within ImageLab,[21] to avoid an over proportional contribution to the values if the denominator is approaching zero or background noise is high. This spectral descriptor is defined by the equation:

$$\mathrm{PHR} = Zb \times \ln(Za/Zb)$$

whereby *Za* and *Zb* are the baseline corrected absorbance intensities of two peaks.

Data analysis

Sparse frequency absorbance datasets were used to create chemical images as follows:

- Collagen map: Peak height ratio of Amide III band (1232 cm^{-1})/collagen CH_2 side chain vibrations (1336 cm^{-1}). The measurement was linear baseline corrected using

intensity values recorded at 1140 and 1356 cm^{-1}. The intensity image produced was mapped against a black-blue (min–max) or white-blue (min–max) colour palette.

• Glycogen map: Peak height ratio of glycogen COH deformation (1028 cm^{-1})/glycogen C–C stretch (1080 cm^{-1}). The measurement was linear baseline corrected using intensity values recorded at 976 and 1180 cm^{-1}. The intensity image produced was mapped against a black-cyan (min–max) colour palette.

• Blue/cyan image: Each chemical map mentioned above was merged into a single blue and cyan colour image.

• *K*-Means, 4 cluster map, using peak height ratio (1232/1336 cm^{-1}) values. This was performed on a 9 × 6 mosaic image recorded using the 4× magnification objective from the whole tissue section. Pixels rejected by the quality test were provided a white colour.

Preliminary analysis was performed on a full band (900–1800 cm^{-1}) dataset recorded using the 12.5× objective. The 3 × 3 mosaic image was analysed using the unsupervised algorithm, *k*-means clustering, a non-hierarchical iterative method that obtains "hard" class membership for each spectrum. A total of 6 clusters was chosen for analysis. A false colour image was constructed, whereby each pixel's cluster membership is defined by a corresponding colour in the image. Pixels rejected by the quality test were provided a black colour. To model the feasibility of recording reduced frequency datasets for tracking fibrosis and glycogen accumulation, peak height ratio images were constructed and fused as described above but using the same full band dataset.

Results and discussion

Fig. 1 describes results obtained from a preliminary analysis of full band spectra recorded from a tissue region displaying typical cirrhotic changes. As is evident in the H&E stained image of 1(a), the normal architecture of the liver is severely degraded in this disease and the liver shows nodules surrounded by fibrous bands. The stain imparts various shades of pink on areas composing hepatocytes or fibrous tissue, and the fibrous bands can be visualised after close scrutiny. The Masson's trichrome stained image displayed in 1(b) provides far greater clarity over the H&E stained image, enabling the examiner to distinguish cells from the surrounding connective tissue. In these images, fibrous tissue is provided a blue colour while the cytoplasm of hepatocytes is stained red. Fig. 1(c) displays a *k*-means infrared spectral clustering image for the equivalent region of unstained tissue. This image was calculated using 6 clusters from a full band (900–1800 cm^{-1}) infrared dataset collected at 1.35 μm pixel resolution from an area 1.95 mm × 1.95 mm in size (3 × 3 mosaic, 2.07 million pixel spectra, 918 MB in size) in a 45 min time period using the 0.7 N.A., 12.5× magnification objective. By direct comparison to the stained images in 1(a–b), the *k*-means image provides similar details and contrast. The fibrous tissue is visualised by the blue and yellow colours, whereas the hepatocytes are described

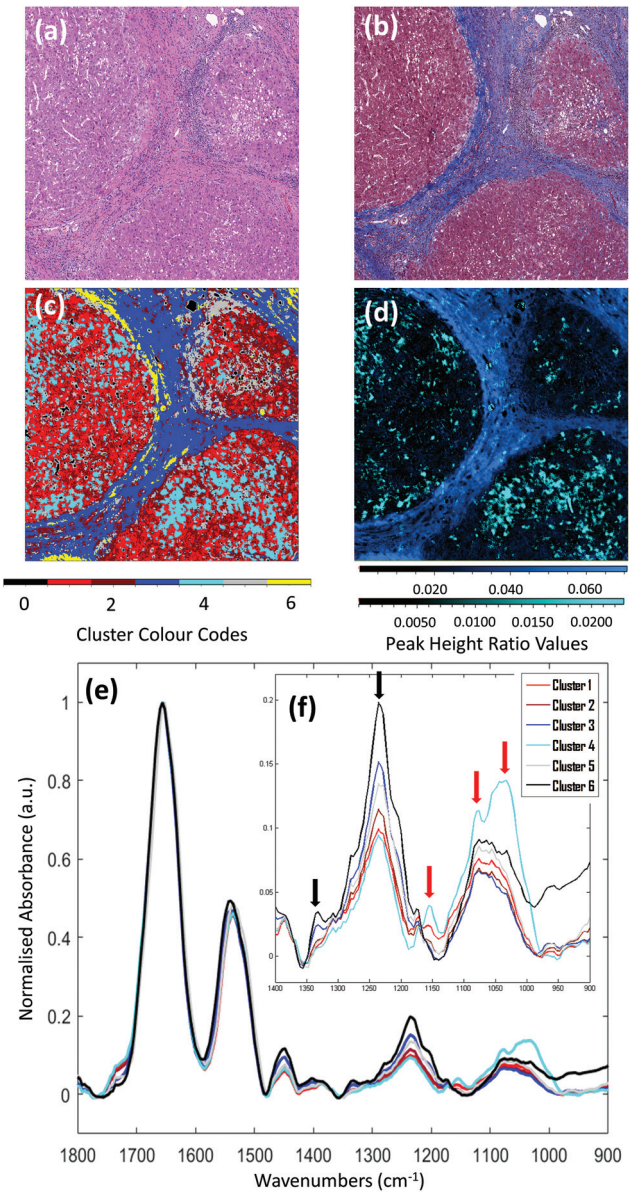

Fig. 1 Spectral staining of a cirrhotic liver tissue section using unsupervised multivariate analysis. (a) Brightfield image of the parallel H&E stained tissue section examined by infrared microscopy. (b) Brightfield image of parallel tissue section stained using the Masson's trichrome protocol. (c) *k*-Means clustering image (6 clusters) calculated from a full band (900–1800 cm^{-1}) infrared absorbance dataset. (d) Fused peak height ratio image calculated using the band ratios (1232/1336 cm^{-1}) and (1028/1080 cm^{-1}), mapped against a black-blue and a black-cyan colour palette respectively. (e)–(f) Mean absorbance spectra calculated for the *k*-means cluster analysis. Bands characteristic of collagen and glycogen have been highlighted by black and red arrows respectively.

by the red and maroon colours. Of note is the cluster of infrared spectra that have been provided the cyan colour and form small clusters within the nodules. After inspection of the mean cluster spectra displayed in Fig. 1(e)–(f), it is clear the pixels provided the cyan colour have contributions from glycogen, displaying characteristic peaks at 1028 (COH deformation), 1080 (C–C stretch) and 1152 (C–O stretch) cm^{-1}

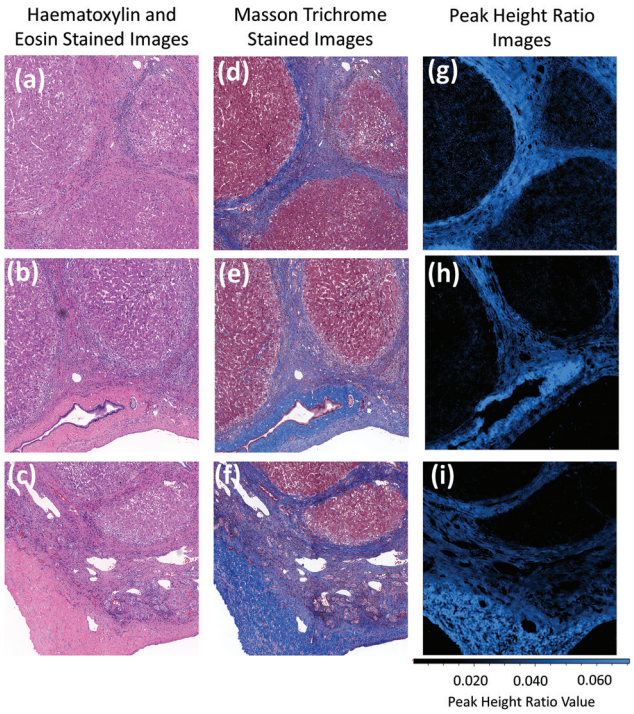

Fig. 2 Mid-infrared based histochemical imaging of liver fibrosis. (a)–(c) Brightfield images of the parallel H&E stained tissue section examined by infrared microscopy. (d)–(f) Brightfield images of parallel tissue section stained using the Masson's trichrome protocol. (g)–(i) Peak height ratio images calculated using the band ratio (1232/1336 cm^{-1}), mapped against a black-blue colour palette respectively.

respectively.[2,13] These bands are highlighted by red arrows in the plot. This is an interesting finding as it provides evidence that mid-infrared imaging has the distinct ability to visualise both reactive fibrosis and glycogen accumulation within liver specimens simultaneously. Mean spectra of the blue and yellow clusters (blue and black in the spectral plot) display strong bands directly associated with collagen, with characteristic strong peaks at 1232 and 1336 cm^{-1} respectively.[2–7] These bands are highlighted by black arrows in the plot. With this information in mind, peak height ratio values were calculated that would provide optimal contrast for the fibrous (1232/1336 cm^{-1}) and glycogenated hepatocytes (1028/1080 cm^{-1}), the results of which are displayed in Fig. 1(d). In this fused ratio image, the ratio values were coloured blue for fibrous tissue and cyan for glycogenated cells. By direct comparison with the Masson's trichrome stained image in Fig. 1(b) there is excellent agreement between the blue hues and reactive fibrosis. By direct comparison of the *k*-means cluster image calculated using the full band spectra in Fig. 1(c), and the band ratio image in Fig. 1(d), we observe strong spatial correlation between pixels assigned with the cyan hue. This lends strong supporting evidence that a simple peak height ratio of bands at 1028 and 1080 cm^{-1} can provide nearly the same information as that provided by a full band spectrum. Follow on work should be conducted to extend the comparison with PAS stained parallel sections. These results provided evidence that fibrosis and glycogen accumulation can be tracked more rapidly using only two peak height ratios of mid-infrared

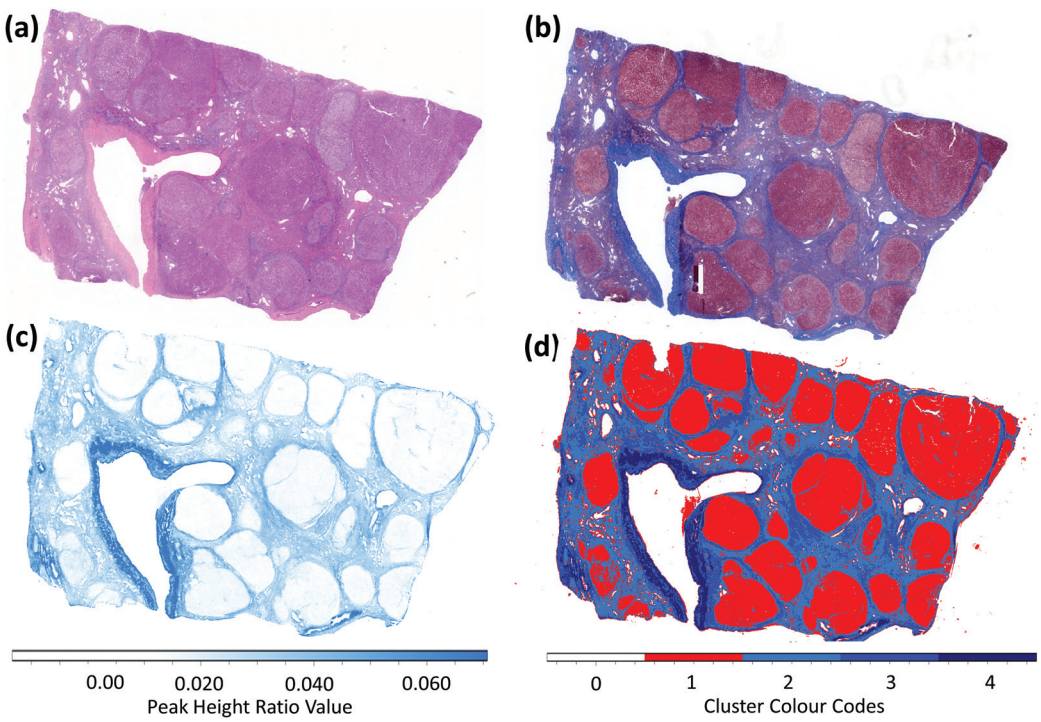

Fig. 3 Mid-infrared based histochemical imaging of a large liver biopsy tissue section (1.8 cm × 1.2 cm in size). (a) Brightfield image of the parallel H&E stained tissue section examined by infrared microscopy. (b) Brightfield image of parallel tissue section stained using the Masson's trichrome protocol. (c) Peak height ratio image calculated using the band ratio (1232/1336 cm^{-1}), mapped against a white-blue colour palette. (d) *k*-Means clustering image (4 clusters) calculated from band ratio values (1232/1336 cm^{-1}) of a 4-frequency infrared absorbance dataset.

bands. Further advancements in QCL instrumentation will enable live imaging of multiple peak height absorbance ratios making it possible to visualise, for example, fibrosis in real-time with very high-contrast on unstained tissue.

Fig. 2 describes results obtained from sparse frequency datasets (3 × 3 mosaics, 2.07 million pixel spectra, 18 MB in size) recorded using the 12.5× magnification objective. These datasets were recorded in 2.7 minutes (*ca.* 16× shorter time and 50× smaller data size than full band datasets of the same mosaic size). These datasets were recorded at 4 targeted wavelengths (1140, 1232, 1336 and 1356 cm^{-1}) found salient for highlighting fibrous tissue. Images were captured from 3 regions of interest that described classic cirrhosis induced structural changes, *i.e.* fibrous banding and nodule formation. Fig. 2(a)–(c) describe the H&E stained images of the tissue regions, whereas Fig. 2(d)–(f) describe Masson's trichrome images of the parallel sections. Images displayed in Fig. 2(g)–(i) show peak height ratio (1232/1336) chemical images of the parallel unstained tissue section. These mid-infrared based chemical images display excellent agreement with the H&E and Masson's trichrome stained images and highlight the reactive fibrosis with distinct clarity as a blue hue.

To assess how rapidly a large tissue biopsy could be imaged and assessed for the degree of fibrosis, a large 9 × 6 sparse frequency mosaic was recorded from the entire liver biopsy section (1.8 cm × 1.2 cm) using the 4× magnification objective of the microscope. This very large dataset composed 12.4 million pixel spectra, was 108 MB in size, and took 16.2 minutes to be collected. Fig. 3 displays results obtained from the analysis of this dataset. Fig. 3(a) and (b) display H&E and Masson trichrome brightfield visible images of the entire tissue section respectively. Fig. 3(c) and (d) display peak height ratio (1232/1336 cm^{-1}) and *k*-means clustering (4 clusters, using peak height ratios calculated in 3(c)) images calculated from the mosaic infrared dataset. At this spatial resolution (*ca.* 12 μm at the protein amide I band) the structure of the fibrotic channels can still be accurately rendered and the infrared chemical images bare good correspondence with their histochemical counterparts.

Conclusions

Special histochemical stains are routinely used in the interpretation of liver biopsies, whether on tumour verses non-tumour cases, or assessment of potential transplant rejection specimens. Masson's trichrome stain is an important stain used in biopsy screening and is predominantly used to assess the degree of fibrosis, which is prevalent in several liver diseases such as hepatitis B and C virus infections, alcoholic liver disease and fatty liver disease. The severity of fibrosis provides hepatologists important information regarding disease stage and aids therapeutic decisions. Comparison of fibrosis is also an important marker to assess the success of any new medications in clinical trials. More recently, the close evaluation of stromal tissue is becoming more important in pathology as there is an increasing understanding that disease processes in multiple organs can change the composition of the adjacent fibrous connective tissue.

The results presented in this contribution lend further evidence to the great promise of QCL infrared microscopy. In this proof of concept study the technology provides a means to acquire chemical images similar to that of routine special histochemical stains with substantial improvements in throughput. Further investigation is required to assess whether these qualitative results can be re-enforced with quantitative metrics useful for pathologists.

Acknowledgements

The authors would like to acknowledge Dr Tim Robbins and Dr Shirley Reidy at SDPathology for sourcing of archival tissue blocks and pathology consult. We would in addition like to thank Dr Hans Lohninger and Elisabeth Renner at Epina for many fruitful conversations and support.

Notes and references

1 J. H. Lefkowitch, *Semin. Diagn. Pathol.*, 2006, (3–4), 190–198.
2 M. J. Romeo, R. K. Dukor and M. Diem, in *Vibrational Spectroscopy for Medical Diagnosis*, ed. M. Diem, P. Griffiths and J. Chalmers, Wiley, Chichester, England, 1st edn, 2008, ch. 1, pp. 1–25 and appendix.
3 M. Guilbert, C. Eklouh-Molinier, K. Wehbe, J. Sulé-Suso, Y. Yang, G. Cinque, P. Jeannesson and G. D. Sockalingum, *J. Biomed. Opt.*, 2014, **19**(11), 111612.
4 R. Chehelatani, J. M. Rosano, B. Wang, A. K. Sabri, N. Pleshko and M. F. Kiani, *J. Biomed. Opt.*, 2012, **17**(5), 056014.
5 K. Lui, A. Man, R. A. Shaw, B. Liang, Z. Xu and Y. Gong, *Biochim. Biophys. Acta*, 2006, **1758**, 960–967.
6 S. Tiwari, V. B. Reddy, R. Bhargava and J. Raman, *PLoS One*, 2015, **10**(5), e0125183.
7 H. Sreedhar, V. K. Varma, F. V. Gambacorta, G. Guzman and M. Walsh, *Biomed. Opt. Express*, 2016, **7**(6), 264021.
8 W. Sun, S. Chang, D. C. S. Tai, N. Tan, G. Xiao, H. Tang and H. Yu, *J. Biomed. Opt.*, 2008, **13**(6), 064010.
9 T. L. Sun, Y. Liu, M. C. Sung, H. C. Chen, C. H. Yang, V. Hovhannisyan, W. C. Lin, Y. M. Jeng, W. L. Chen, L. L. Chiou, G. T. Huang, K. H. Kim, P. T. So, Y. F. Chen, H. S. Lee and C. Y. Dong, *J. Biomed. Opt.*, 2010, **15**(3), 036002.
10 L. Gailhouste, Y. Le Grand, C. Odin, D. Guyader, B. Turlin, F. Ezan, Y. Desille, T. Guilbry, A. Bessard, C. Fremin, N. B. Theret and G. Baffet, *J. Hepatol.*, 2010, **52**, 398–406.
11 K. D. Fairbanks and A. S. Tavill, *Am. J. Gastroenterol.*, 2008, **103**(8), 2136–2141.
12 A. Qizilbash and O. Young-Pong, *Am. J. Clin. Pathol.*, 1983, **79**(6), 697–702.
13 M. J. Romeo, B. R. Wood and D. McNaughton, *Vib. Spectrosc.*, 2002, **28**(1), 167.

14 N. Kroger-Lui, N. Getz, K. Hasse, B. Kranzlin, S. Neudecker, A. Pucci, A. Regenscheit, A. Schonhals and W. Petrich, *Analyst*, 2015, **140**, 2086.
15 L. G. Luna, *Manual of Histologic Staining Methods of the Armed Forces Institute of Pathology*, McGraw-Hill, NewYork, 1968.
16 N. C. Foot, *Stain Technol.*, 1933, **8**(3), 101–110.
17 P. Bassan, M. J. Weida, J. Rowlette and P. Gardner, *Analyst*, 2014, **139**, 3856–3859.
18 M. J. Pilling, A. Henderson, B. Bird, M. D. Brown, N. W. Clarke and P. Gardner, *Faraday Discuss.*, 2016, **187**, 135–154.
19 C. Hughes, G. Clemens, B. Bird, T. Dawson, K. M. Aston, M. D. Jenkinson, A. Brodbelt, M. Weida, E. Fotheringham, M. Barre, J. Rowlette and M. J. Baker, *Sci. Rep.*, 2016, **6**, 20173.
20 K. Yeh, S. Kenkel, J. Lui and R. Bhargava, *Anal. Chem.*, 2015, **87**(1), 485–493.
21 Epina GmbH, Austria, 2016, http://www.imagelab.at.
22 A. A. Green, M. Berman, P. Switzer and M. D. Craig, *IEEE Trans. Geosci. Remote Sens.*, 1988, **26**, 65–74.
23 P. H. C. Eilers and H. F. M. Boelens, Technical report, Leiden University Medical Center, 2005.

